Lawrence Berkeley National Laboratory

Recent Work

Title

Enhanced Electrochemical Methanation of Carbon Dioxide with a Dispersible Nanoscale Copper Catalyst

Permalink

https://escholarship.org/uc/item/4882v99t

Journal

Journal of the American Chemical Society, 136(38)

ISSN

0002-7863

Authors

Manthiram, Karthish
Beberwyck, Brandon J.
Alivisatos, A. Paul

Publication Date

2014-09-24

eScholarship.org Powered by the California Digital Library
University of California

Enhanced Electrochemical Methanation of Carbon Dioxide with a Dispersible Nanoscale Copper Catalyst

Karthish Manthiram[†⊥∥], **Brandon J. Beberwyck**[‡⊥∥], **and A. Paul Alivisatos***[§⊥∥]

[†]Department of Chemical and Biomolecular Engineering, [‡]Department of Materials Science and Engineering, [§]Department of Chemistry, and [⊥]Kavli Energy Nanosciences Institute, University of California, Berkeley, California 94720, United States

[∥] Materials Sciences Division, Lawrence Berkeley National Laboratory, Berkeley, California 94720, United States

DOI: 10.1021/ja5065284

alivis@berkeley.edu

•

Abstract

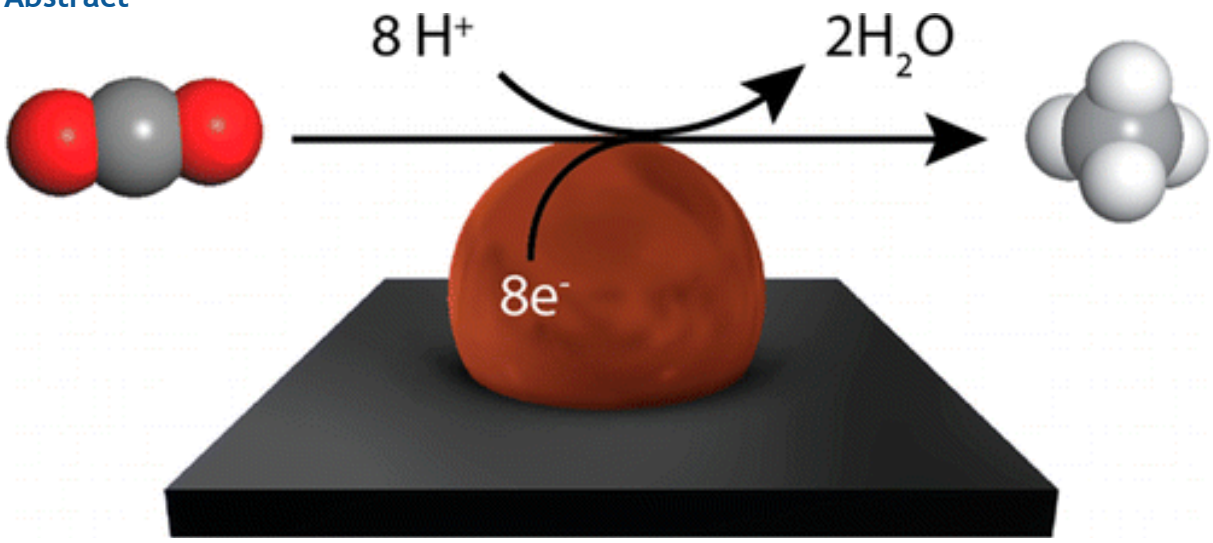

Although the vast majority of hydrocarbon fuels and products are presently derived from petroleum, there is much interest in the development of routes for synthesizing these same products by hydrogenating CO_2. The simplest hydrocarbon target is methane, which can utilize existing infrastructure for natural gas storage, distribution, and consumption. Electrochemical methods for methanizing CO_2 currently suffer from a combination of low activities and poor selectivities. We demonstrate that copper nanoparticles supported on glassy carbon (n-Cu/C) achieve up to 4 times greater methanation current densities compared to high-purity copper foil electrodes. The n-Cu/C electrocatalyst also exhibits an average Faradaic efficiency for methanation of 80% during extended

electrolysis, the highest Faradaic efficiency for room-temperature methanation reported to date. We find that the level of copper catalyst loading on the glassy carbon support has an enormous impact on the morphology of the copper under catalytic conditions and the resulting Faradaic efficiency for methane. The improved activity and Faradaic efficiency for methanation involves a mechanism that is distinct from what is generally thought to occur on copper foils. Electrochemical data indicate that the early steps of methanation on n-Cu/C involve a pre-equilibrium one-electron transfer to CO_2 to form an adsorbed radical, followed by a rate-limiting non-electrochemical step in which the adsorbed CO_2 radical reacts with a second CO_2 molecule from solution. These nanoscale copper electrocatalysts represent a first step toward the preparation of practical methanation catalysts that can be incorporated into membrane-electrode assemblies in electrolyzers.

•

Introduction

The conversion of CO_2 into hydrocarbons is an alternative route for synthesizing fuels and feedstocks that are typically derived from oil or natural gas, representing one potential strategy to store electrical energy derived from intermittent sources of clean energy, such as wind and solar.(1, 2) Although electrosynthetic pathways for converting CO_2 into hydrocarbon products are not economically feasible at present,(3) expected decreases in the price of electricity derived from clean energy sources(4) and policy changes regarding greenhouse gas emissions(5) may alter the economics of reducing CO_2 dramatically. In fact, growing use of intermittent renewable energy sources in certain regions has accelerated the deployment of small-scale electrical energy storage systems, including pilot plants for methanizing CO_2.(6) These pilot plants utilize a two-step process, in which electrical energy is used to power an electrolyzer that splits water to produce hydrogen and oxygen. The hydrogen is then used in the Sabatier reaction,(7) in which CO_2 and H_2 are reacted over a heterogeneous nickel catalyst at temperatures of 250–400 °C and pressures of 1–80 bar to produce methane, which can be injected into existing natural gas networks. A single-step electrochemical process that can directly convert CO_2 to methane under conditions of ambient pressure and temperature may represent an attractive alternative.

Of the metals explored as catalysts for electrochemical CO_2 reduction,(8) the most active and selective identified to date are gold, silver, and bismuth,(9-14) which produce CO as their terminal product. Copper is attractive in comparison, as it produces more reduced hydrocarbon products.(8, 15-17) One of the hydrocarbon products formed on copper electrocatalysts is methane, which forms through the following half-reaction:

$$CO_2 + 8H^+ + 8e^- \rightarrow CH_4 + 2H_2O \quad (1)$$

Because the reaction involves eight electron-transfer steps at 0.17 V (all potentials reported versus reversible hydrogen electrode (RHE)) that can easily bifurcate to form a wide range of products, the process exhibits poor selectivity for any single product, forming a mixture of methane, ethylene, hydrogen, carbon monoxide, and formic acid.(18, 19) The highest Faradaic efficiencies for methane reported to date are 64% on a (210) copper single crystal(18, 20) and 73% on an electrodeposited copper electrode.(21) Although studies conducted on high-purity foils, single crystals, and electrodeposited materials have served as useful benchmarks and provide fundamental insights into how copper catalyzes the reduction of CO_2, these model materials are impractical for electrolyzers as they have low surface areas, cannot be incorporated into the membrane electrode assemblies(22) that are needed to achieve high current densities with low ionic resistances, or are expensive. From the point of view of cost and ease of manufacturing, highly dispersed nanoparticle catalysts are much better suited for electrolyzers.(23) Here, we demonstrate that well-dispersed copper nanoparticles supported on glassy carbon show high activities and Faradaic efficiencies for methanation, comparable to those of much more expensive single-crystal electrodes. Systematic studies of nanoparticle loading on the glassy carbon support and electrochemical analysis indicate that the altered reactivity of the copper nanoparticles is due to distinct catalytic sites present on isolated nanoparticle catalysts supported on glassy carbon.

•

Results and Discussion

We colloidally synthesized copper nanoparticles capped with tetradecylphosphonate of diameter 7.0 ± 0.4 nm (Figure 1A,B).(24) These particles were spin-coated onto glassy carbon plates (Figure 1C), hereafter referred to as n-Cu/C, which served as the working electrode in a three-electrode setup containing CO_2-saturated 0.1 M sodium bicarbonate electrolyte, pH 6.8. As a control, we also used high-purity copper foils as the working electrode. All current densities for nanoparticle electrodes are surface-area normalized.

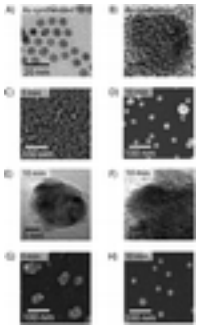

Figure 1. Morphological evolution of copper nanoparticles during the course of electrochemical CO_2 reduction. Transmission electron microscopy (TEM) images

of as-synthesized copper nanoparticles of diameter 7.0 ± 0.4 nm at (A) low magnification and (B) high magnification, showing that the initial particles are highly polycrystalline. (C) Scanning electron microscopy (SEM) of n-Cu/C electrode, consisting of copper nanoparticles supported on glassy carbon substrate. (D) SEM of the same n-Cu/C electrode following polarization for 10 min at −1.25 V under CO_2 electroreduction conditions, demonstrating that the average particle diameter grows to 23 ± 8 nm. TEM images of copper nanoparticle transferred from glassy carbon substrate onto TEM grid at (E) low magnification and (F) high magnification, in which it is evident that the particles that form under polarization are highly polycrystalline. (G) SEM of trimethylsilyl chloride-treated n-Cu/C electrode prior to polarization, in which particles have an average diameter of 52 ± 21 nm. (H) SEM of the same electrode following polarization for 10 min at −1.25 V, in which the particles that form are 25 ± 8 nm in diameter.

Morphological Evolution

During the course of electrochemical CO_2 reduction, the morphology of the copper nanoparticles changes significantly, growing in size to 23 ± 8 nm in diameter (Figure 1D). The nanoparticles that form are highly polycrystalline, as revealed using high-resolution transmission electron microscopy (HR-TEM, Figure 1E,F). We find that irrespective of the initial size of the nanoparticles on glassy carbon, the particles evolve in size to form particles which are ~25 nm in diameter, even if we begin with larger particles. For instance, if we treat the initially cast particles (Figure 1C) with trimethylsilyl chloride, the tetradecylphosphonate ligand is stripped off of the surface of the particles, causing the particles to ripen to a diameter of 52 ± 21 nm prior to polarization (Figure 1G). These large, irregular particles then evolve in size and shape during the course of electrochemical CO_2 reduction to form smaller, uniform, roughly spherical particles which are 25 ± 8 nm in diameter (Figure 1H). Similar changes in size are also observed in the absence of CO_2 (Figure S1). The morphological evolution observed, which may be due to a combination of particle coalescence and dissolution–redeposition, points toward the importance of verifying if size distributions are maintained in studies of size-dependent electrocatalysis.(25)

Catalytic Behavior

Although the n-Cu/C electrodes and copper foil electrodes exhibit comparable current densities at lower overpotentials, the current densities for n-Cu/C electrodes are over twice as high at more reducing potentials (Figure 2A). Of this increased current, a much greater fraction from the n-Cu/C electrode goes toward methane compared to the copper foil (Figure 2B). The Faradaic efficiency for methane is improved at more reducing potentials for n-Cu/C, reaching 76% at −1.35 V. This is significantly higher than the Faradaic efficiency of 44% achieved on a polycrystalline copper foil at the same potential (Figure 2B). The combined enhancement in both the overall current density and Faradaic efficiency for methanation on n-Cu/C leads to partial current densities for methane that are four times higher for n-Cu/C compared to the copper foil at −1.35 V (Figure 2C).

Hydrogen evolution, which is undesirable since the intended reduction target is CO_2, is also suppressed on n-Cu/C compared to the copper foil. The Faradaic efficiency for hydrogen is 13% at −1.25 V on n-Cu/C, half that of a polycrystalline copper foil at the same potential (Figure 2D).

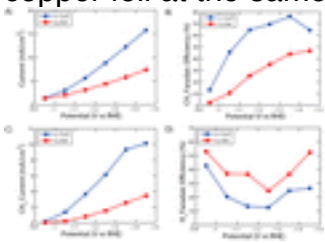

Figure 2. Comparison of current densities and Faradaic efficiencies for n-Cu/C and copper foil electrodes. (A) Total current density, demonstrating that n-Cu/C has greater overall reduction activity than the copper foil. (B) Faradaic efficiency for methane, in which it is evident that n-Cu/C is more selective for methane than the copper foil. (C) Methanation current density, in which the combined effect of the improved current density and Faradaic efficiency on n-Cu/C is apparent. (D) Faradaic efficiency for hydrogen as a function of potential, showing suppressed hydrogen evolution on the n-Cu/C catalyst.

The current densities for n-Cu/C are relatively stable at −1.25 V during extended periods of CO_2 reduction (Figure 3A), decaying only 3% over the course of 1 h, indicating a stability surpassing copper foil electrodes, for which the current density decays by 11% (Figure S2). The Faradaic efficiency for methane on n-Cu/C does not decay during extended periods of CO_2 reduction (Figure 3B), remaining in the range of 71–90%, with an average yield of 80% over 1 h, which is the highest Faradaic efficiency for methanation reported to date.

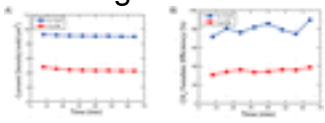

Figure 3. Stability of the n-Cu/C and copper foil catalysts. (A) Total current density and (B) Faradaic efficiency for methanation as a function of time for both n-Cu/C and copper foil polarized at −1.25 V, demonstrating that the n-Cu/C catalyst is stable.

Continuum from Nanoparticle-like to Foil-like Behavior

There are many structural, morphological, and chemical differences between the copper nanoparticles supported on glassy carbon and copper foil electrodes, which could hypothetically be responsible for the increased Faradaic efficiencies for methanation. Some sources of the differences include the presence of tetradecylphosphonate ligand capping the nanoparticles and impurities present in the initial nanoparticles, since they are prepared from a 97% pure copper precursor. In order to determine the effect of these various factors, we utilized a distinctly different method of preparation of the electrocatalyst, by evaporating a thin film of copper onto glassy carbon using a high-purity copper source. For a 3

nm film (Figure 4A), we find that a Faradaic efficiency for methanation of 76% can be achieved (Figure 4E), allowing us to conclusively exclude the possibility that the presence of ligands and impurities in the starting material influence the observed improvement in Faradaic efficiency for methanation on n-Cu/C.

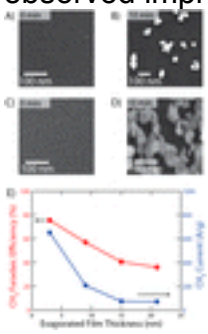

Figure 4. Continuum of catalytic behavior between nanoparticle-like and foil-like electrodes: 3 nm evaporated copper film (A) prior to and (B) following polarization at −1.25 V for 10 min, and 15 nm evaporated copper film (C) prior to and (D) following polarization at −1.25 V for 10 min. (E) Methanation Faradaic efficiency and gravimetric methanation current as a function of evaporated copper film thickness, from which it is evident that thin evaporated films behave like the n-Cu/C electrodes while thick evaporated films behave like copper foils.

The thickness of the initially evaporated copper film has a dramatic impact on the Faradaic efficiency for methane. Evaporated films that are relatively thin (Figure 4A) produce isolated nanoscale aggregates upon polarization on the electrode (Figure 4B) which somewhat resemble the n-Cu/C electrodes (Figure 1D); these electrodes have high methanation yields (Figure 4E). In contrast, thicker films (Figure 4C) produce highly connected networks of fused nanoparticles upon polarization (Figure 4D); these electrodes have low Faradaic efficiencies for methanation (Figure 4E), as we would expect for an architecture that resembles a polycrystalline foil. This possibly explains why previous studies of dense films of copper nanoparticles have not observed enhanced methanation yields.(26-28) A systematic study of single-crystal electrodes for CO_2 reduction has put forth the possibility that the introduction of a particular step-edge present on a (210) single crystal can enhance methanation yields.(20) This suggests that more isolated nanoparticles expose catalytic sites that are more effective for methanation, which are lost as they fuse to form dense aggregates. Structural differences have also been implicated in the enhanced selectivity for CO observed on copper foil catalysts which are oxidized and then reduced.(27, 29) Our results demonstrate a continuum of catalytic behavior that exists between electrodes that exhibit nanoparticle-like and foil-like behavior, and that this behavior can be systematically tuned by adjusting the mass loading of copper on glassy carbon (Figure 4E).

Mechanism

In order to glean mechanistic insights regarding the altered catalytic behavior of n-Cu/C compared to copper foils, we measured the Tafel slope of the n-Cu/C

catalyst. In the region of Tafel linearity, the Tafel slope for methanation is 60 ± 4.2 mV/decade for n-Cu/C (Figure 5A), close to a value of 59 mV/decade, indicative of a one-electron pre-equilibrium step prior to a rate-limiting non-electrochemical step.(11, 12, 30, 31) Tafel slopes for methanation on copper foils vary widely depending on surface preparation, ranging from as low as 86 ± 4.6 mV/decade (Figure 5A) to as high as 175 mV/decade.(32) It is generally thought that the rate-limiting step for methanation on copper foils involves a single electron transfer to CO_2 on copper foils,(18) which would correspond to a Tafel slope of 120 mV/decade. The reduced Tafel slope on n-Cu/C is advantageous because smaller excursions in potential are needed to drive logarithmic gains in methanation current.

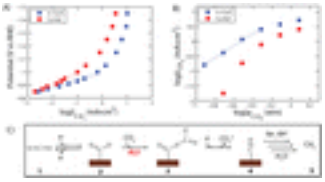

Figure 5. Mechanistic insights from Tafel analysis. (A) Tafel plot for n-Cu/C and copper foil, with linear fit at low current densities demonstrating that these catalysts have Tafel slopes of 60 ± 4.2 and 86 ± 4.6 mV/decade, respectively. The Tafel slope for n-Cu/C indicates a one electron pre-equilibrium step precedes a non-electrochemical rate-limiting step. (B) Methanation current density as a function of partial pressure of CO_2 at −1.25 V, demonstrating that methanation current density has a 2.03 ± 0.08 order dependence on the partial pressure of CO_2 at lower CO_2 partial pressures. (C) Proposed mechanism for the electrochemical reduction of CO_2 to methane, including the rate-limiting step (RLS). This mechanism is consistent with the gathered electrochemical data and known intermediates for CO_2 reduction that have been identified in the literature.

While the Tafel slope provides general insights into the nature of the possible rate-limiting and pre-equilibrium steps, the order dependence of the methanation current on reactants provides a more detailed picture of the rate-limiting step. We find an unusual second-order (2.03 ± 0.08) dependence of methanation current on CO_2 partial pressure for the n-Cu/C catalyst (Figure 5B).(33) Based on work on other metals, such as gold(9) and mercury,(34) it is often assumed that CO_2 reduction on copper foils proceeds with a first-order dependence on CO_2 in aqueous electrolytes,(35, 36) although we observe an ill-defined order (Figure 5B). The methanation current on the n-Cu/C catalyst exhibits no clear order dependence on sodium bicarbonate concentration (Figure S3), although optimization of the buffer concentration can further enhance Faradaic efficiencies for methanation by approximately 10% (Supporting Information).

Combining the insights provided by the preceding electrochemical analysis, we propose early steps in a possible mechanism that could lead to methane formation (Figure 5C). In this proposed mechanism, the CO_2 **1** reacts in a one-

electron-transfer pre-equilibrium step to form a surface adsorbed CO_2 radical **2**. The CO_2 radical has been experimentally observed on other metals, and it is inferred that it also forms on copper.(18, 34, 37, 38) If we assume that the surface coverage of the CO_2 radical $\theta \ll 1$, consistent with the observation that copper surfaces are predominantly covered in CO under CO_2 reduction conditions,(39-41) then θ is related to the overpotential η and CO_2 partial pressure p_{CO2} as

$$\theta = K_1 p_{CO_2} \exp\left(\frac{F\eta}{RT}\right) \quad (2)$$

where K_1 is the equilibrium constant for the conversion of **1** to **2**, F is Faraday's constant, R is the gas constant, and T is temperature (Supporting Information).(30) Following the pre-equilibrium step, the adsorbed CO_2 radical **2** is proposed to undergo rate-limiting carbon–oxygen coupling with a Lewis acid CO_2 molecule from solution to form a CO_2–$CO_2^{-\bullet}$ adduct **3**, which could be either a transition state or a genuine intermediate. Such an adduct has been postulated for electrochemical reduction of CO_2 in non-aqueous solvents on other metals.(38, 42-44) The rate of the CO_2–$CO_2^{-\bullet}$ adduct formation step, expressed as a methanation current, is

$$i_{CH_4} = nFk_2 p_{CO_2} \theta \quad (3)$$

where n is the total number of electron transfers needed to convert CO_2 **1** to methane **5** and k_2 is the rate constant for the conversion of **2** to **3**. Combining eqs 2 and 3, we obtain

$$i_{CH_4} = nFk_2 K_1 p_{CO_2}^2 \exp\left(\frac{F\eta}{RT}\right) \quad (4)$$

This rate law is consistent with the second-order dependence on CO_2 partial pressure that we experimentally observe. The Tafel slope is given by the partial derivative of the overpotential η with respect to the logarithm of current,(30) which we apply to eq 4, yielding

$$\left(\frac{\partial \eta}{\partial \log i_{CH_4}}\right)_{P_{CO_2}} = \frac{2.3RT}{F} = 59 \text{ mV/decade} \quad (5)$$

Hence, the theoretical Tafel slope of 59 mV/decade for the proposed mechanism is consistent with our experimental measurement of a 60 ± 4.2 mV/decade (Figure 5A). The preceding analysis involving the Tafel slope and order-dependence on p_{CO2} has also allowed us to exclude several alternative mechanisms, such as the self-coupling of two $CO_2^{-\bullet}$ and rate-limiting electron

transfer to CO_2 (Supporting Information).

Based on mechanistic understanding of CO_2 reduction on other metals, we may also propose downstream steps for the conversion of CO_2–$CO_2^{-\bullet}$ into methane. In studies done on mercury and lead in dimethylformamide,(38, 42-44) the CO_2–$CO_2^{-\bullet}$ adduct **3** is believed to reductively disproportionate to yield both CO_3^{2-} and CO, which is a terminal product on these electrodes. Our experimental observation of CO as a minor product on n-Cu/C electrodes (Figure S4) is consistent with its appearance as an intermediate in our proposed mechanism. Given CO is known to bind to copper with an adsorption enthalpy of ~20 kcal/mol,(45) we may expect it to bind to the copper and further react. The downstream steps in which the adsorbed CO molecule **4** reacts to form methane **5** may be similar to what has been previously proposed for copper foil electrodes based on detailed studies of their reactivity with CO.(36, 46)

•

Conclusion

These nanoscale copper electrocatalysts represent a first step toward the development of a dispersed electrochemical methanation catalyst that can be used in practical electrolyzers.(22) Copper nanoparticles are ideal for preparing gas diffusion layers for membrane-electrode assemblies which minimize polarization losses, maximizing the energy efficiency of electrolyzers. In addition, these colloidally prepared copper nanoparticles have catalytic properties that rival those of much more expensive high-purity foils and single-crystal electrodes. The finding of improved methanation activity and Faradaic efficiency for copper nanoparticle catalysts on glassy carbon through a unique mechanism paves the way for complementary computational and spectroscopic studies to develop a more detailed mechanistic understanding of the origin of the improved catalytic properties.

•

Experimental Methods

Synthesis of Copper Nanoparticles

Copper nanoparticles capped with tetradecylphosphonate and suspended in hexane were synthesized following a literature method.(24) Briefly, 10 mL of trioctylamine (Sigma-Aldrich, 98%) was heated in a 25 mL three neck flask equipped with a condenser and stir bar to 130 °C under argon for 1 h in order to dry the solvent. The trioctylamine was then cooled to room temperature; while keeping the flask purged with argon, 123 mg of copper(I) acetate (Sigma-Aldrich, 97%) and 139 mg of *n*-tetradecylphosphonic acid (TCI Synthesis, Lot No. 808002N09) were added to the trioctylamine. The solution was then rapidly heated to 180 °C under argon, swirled briefly to release any precursors adhered to the walls of the flask, and kept at this temperature for 30 min. The solution was

rapidly heated to 270 °C and held at that temperature for 30 min. After cooling to room temperature, the copper particles were removed using air-free techniques and transferred to a glovebox. Just prior to electrode fabrication, 0.15 mL of the as-synthesized particles in trioctylamine was diluted with 0.75 mL of hexane, and then precipitated by adding 1.4 mL of isopropanol, under air-free conditions. The particles were separated by centrifuging at 8000 rpm for 8 min. The solvent was decanted under ambient conditions, and the particles were resuspended in 1 mL of hexane by vortexing. The volume of hexane in which the particles are resuspended can be changed in order to optimize the particle loading on glassy carbon; this is critical for achieving high methanation yields.

Fabrication of n-Cu/C Electrodes

Glassy carbon plates (Type 2, Alfa Aesar) with 5.2 cm^2 of active surface area were polished using 1 μm alpha alumina (CH Instruments) and 50 nm gamma alumina (CH Instruments). The plates were rinsed with Milli-Q water, sonicated briefly, and blown dry with nitrogen. 600 μL of copper nanoparticles suspended in hexane were deposited on the substrate, which was then spun at 1000 rpm on a spin-coater for 60 s. 600 μL of ethanol was deposited on the substrate, which was allowed to sit for 30 s, and then spun at 1000 rpm for 60 s. Then, for trimethylsilyl chloride-treated electrodes, the substrate was covered in 600 μL of 2 wt % trimethylsilyl chloride in hexane and spun at 1000 rpm for 60 s, which was repeated once; then, the substrate was covered in 600 μL of ethanol and spun at 1000 rpm for 60 s, which was also repeated once.

Fabrication of Evaporated Copper Electrodes

Glassy carbon plates were polished as described above. A thermal evaporator (Edwards Auto 500, FTM7) in an argon glovebox was used to evaporate copper films on the glassy carbon, using a high-purity copper source (99.9999%, Alfa Aesar). The films ranged in thickness from 3 to 21 nm, as measured using a quartz crystal monitor, and were deposited at a rate of approximately 3 nm/min. The plates were transferred under ambient conditions for use in the electrochemical cell.

Preparation of Copper Foil Electrodes

High-purity copper foils were wet-sanded using 1500 grit sandpaper (Norton Blackice), rinsed with Milli-Q water, dipped in 8% nitric acid for 30 s, rinsed again with Milli-Q water, and then blown dry with nitrogen.

Microscopy of Electrodes

As synthesized copper nanoparticles were imaged by drop-casting on a TEM grid (Electron Microscopy Sciences, CF-400-Cu) and acquiring images on a 200 kV Tecnai G2 20 S-TWIN with a Gatan SC200 CCD camera. After polarization, glassy carbon electrodes were rinsed with Milli-Q water and blown dry with nitrogen. Particles were transferred from the glassy carbon electrode to a TEM grid by placing a grid on top of the electrode and applying pressure to the grid using a glass microscope slide for a few seconds. SEM images of electrodes were acquired using a Zeiss Ultra 55 field emission scanning electron microscope with an InLens detector, 5 kV accelerating voltage, and 5 mm

working distance.

Electrochemical Methods

Electrochemical measurements were conducted in a two-compartment electrochemical flow cell fabricated from polychlorotrifluoroethylene (Kel-F), similar to a design used in the literature.(19) The working electrode compartment and counter electrode compartment, which each had an electrolyte volume of 5 mL and a gas headspace of ~1 mL, were separated by a Selemion membrane (AMV, AGC Engineering). A Ag/AgCl reference electrode (BASi, RE-6), which was stored in saturated KCl when not in use, was used; all measured potentials were converted to the RHE scale. The current densities measured for nanoparticle electrodes were normalized by the copper surface area; the surface area was determined by measuring the diameter of particles using SEM and calculating their surface area by treating them as spheres. For copper foils, the geometric surface areas were used, such that the reported current densities serve as upper bounds for the activity of copper foils. 0.1 M $NaHCO_3$ in Milli-Q water was used as the electrolyte, which was prepared by bubbling CO_2 (Praxair, CD M-50, >99%) through a solution of half the molarity of Na_2CO_3 (99.9999%, Sigma-Aldrich), producing a solution of pH 6.8 after approximately 2 h. The electrochemical cell was continuously purged with CO_2 at a flow rate of 20 mL/min and a pressure of 1.2 atm; cells were purged for at least 5 min following assembly and before electrochemical polarization. For the experiments where CO_2 partial pressure was varied, the total flow rate and pressure of CO_2 were kept constant, while adding in a diluent stream of argon. Potentiostatic experiments were conducted by stepping to the desired potential, holding at that potential for 10 min, and sending a sample to the gas chromatograph (SRI Instruments, MG #3 Configuration) at the end of the 10 min interval. The gas chromatograph was equipped with TCD and FID detectors, a methanizer, and Molsieve 13x and Hayesep D columns.

Supporting Information

Additional electrochemical data on electrode stability, order dependence, and mechanistic insights. This material is available free of charge via the Internet at http://pubs.acs.org.

The authors declare no competing financial interest.

•

Acknowledgment

We thank Virginia Altoe, David Barton, Alex Bell, Trevor Ewers, Eric Granlund, Prashant Jain, Kendra Kuhl, Bryan McCloskey, Pete Nickias, Phillip Ross, Rachel Segalman, Yogesh Surendranath, and Mark Yoshida for useful discussions. This work was supported by the Dow Chemical Co. under contract 20120984. SEM was conducted at the Molecular Foundry, supported by the Office of Science, Basic Energy Sciences, of the U.S. Department of Energy under contract DE-AC02-05CH11231. K.M. gratefully acknowledges the support

from the U.S. Department of Energy Office of Science Graduate Fellowship. A.P.A. was supported by the U.S. Department of Energy under contract DE-AC02-05CH11231.

- Reference QuickView
-

References

This article references 46 other publications.

1. Nocera, D. G. *ChemSusChem* **2009**, 2, 387[CrossRef], [PubMed], [CAS]
2. Lewis, N.; Nocera, D. *Proc. Natl. Acad. Sci. U.S.A.* **2006**, 104, 15729[Free @ PNAS], [CrossRef]
3. Banholzer, W.; Jones, M. *AIChE J.* **2013**, 59, 2708[CrossRef], [CAS]
4. Reichelstein, S.; Yorston, M. *Energy Policy* **2013**, 55, 117[CrossRef]
5. *Climate Change 2014: Mitigation of Climate Change*; Intergovernmental Panel on Climate Change: Geneva, **2014**.
6. Schiebahn, S.; Grube, T.; Robinus, M.; Zhao, L.; Otto, A.; Kumar, B.; Weber, M.; Stolten, D. In *Transition to Renewable Energy Systems*; Stolten, D.; Scherer, V., Eds.; Wiley: Weinheim, Germany, **2013**; pp 813–847.[CrossRef]
7. Sabatier, P.; Senderens, J. B. *C. R. Acad. Sci.* **1902**, 134, 689[CAS]
8. Hori, Y.; Kikuchi, K.; Suzuki, S. *Chem. Lett.* **1985**, 11, 1695[CrossRef]
9. Hori, Y.; Murata, A.; Kikuchi, K.; Suzuki, S. *J. Chem. Soc., Chem. Commun.* **1987**, 728[CrossRef], [CAS]
10. Zhu, W.; Michalsky, R.; Metin, O.; Lv, H.; Guo, S.; Wright, C. J.; Sun, X.; Peterson, A. A.; Sun, S. *J. Am. Chem. Soc.* **2013**, 135, 16833ACS Full Text, [PubMed], [CAS]
11. Lu, Q.; Rosen, J.; Zhou, Y.; Hutchings, G. S.; Kimmel, Y. C.; Chen, J. G.; Jiao, F. *Nat. Commun.* **2014**, 5, 3242[CrossRef], [PubMed], [CAS]
12. Chen, Y.; Li, C. W.; Kanan, M. W. *J. Am. Chem. Soc.* **2012**, 134, 19969ACS Full Text, [PubMed], [CAS]
13. DiMeglio, J. L.; Rosenthal, J. *J. Am. Chem. Soc.* **2013**, 135, 8798ACS Full Text, [PubMed], [CAS]
14. Medina-Ramos, J.; Dimeglio, J. L.; Rosenthal, J. *J. Am. Chem. Soc.* **2014**, 136, 8361ACS Full Text, [PubMed], [CAS]
15. Hori, Y.; Murata, A.; Takahashi, R. *J. Chem. Soc., Faraday Trans.* **1989**, 85, 2309[CrossRef], [CAS]
16. Peterson, A. A.; Abild-Pedersen, F.; Studt, F.; Rossmeisl, J.; Nørskov, J. K. *Energy Environ. Sci.* **2010**, 3, 1311[CrossRef], [CAS]
17. Peterson, A.; Nørskov, J. *J. Phys. Chem. Lett.* **2012**, 2, 251[ACS Full Text]
18. Hori, Y. In *Modern Aspects of Electrochemistry*; Vayenas, C. G.; White, R. E.; Gamboa-Aldeco, M. E., Eds.; Springer: New York, **2008**; pp 89– 189.[CrossRef]

19. Kuhl, K. P.; Cave, E. R.; Abram, D. N.; Jaramillo, T. F. *Energy Environ. Sci.* **2012**, 5, 7050[CrossRef], [CAS]
20. Hori, Y.; Takahashi, I.; Koga, O.; Hoshi, N. *J. Phys. Chem. B* **2002**, 106, 15[ACS Full Text], [CAS]
21. Cook, R.; MacDuff, R.; Sammells, A. *J. Electrochem. Soc.* **1988**, 135, 1320[CrossRef], [CAS]
22. Weidner, J. W.; Sethuraman, V. A.; Van Zee, J. W. *Interface* **2003**, 12, 40
23. Rand, D.; Dell, R. *Hydrogen Energy: Challenges and Prospects*, 1st ed.; Hunt, J., Ed.; RSC Publishing: Cambridge, **2007**.
24. Hung, L.-I.; Tsung, C.-K.; Huang, W.; Yang, P. *Adv. Mater.* **2010**, 22, 1910[CrossRef], [PubMed], [CAS]
25. Manthiram, K.; Surendranath, Y.; Alivisatos, A. P. *J. Am. Chem. Soc.* **2014**, 136, 7237ACS Full Text, [PubMed], [CAS]
26. Tang, W.; Peterson, A.; Varela, A. *Phys. Chem. Chem. Phys.* **2012**, 4, 76[CrossRef]
27. Li, C. W.; Kanan, M. W. *J. Am. Chem. Soc.* **2012**, 134, 7231ACS Full Text, [PubMed], [CAS]
28. Reske, R.; Mistry, H.; Behafarid, F.; Roldan Cuenya, B.; Strasser, P. *J. Am. Chem. Soc.* **2014**, 136, 6978ACS Full Text, [PubMed], [CAS]
29. Li, C. W.; Ciston, J.; Kanan, M. W. *Nature* **2014**, 508, 504[CrossRef], [PubMed], [CAS]
30. Gileadi, E. *Physical Electrochemistry: Fundamentals, Techniques and Applications*, 1st ed.; Wiley-VCH: Weinheim, Germany, **2011**.
31. Chen, Y.; Kanan, M. W. *J. Am. Chem. Soc.* **2012**, 134, 1986ACS Full Text, [PubMed], [CAS]
32. Kim, J. J.; Summers, D. P.; Frese, K. W. *J. Electroanal. Chem.* **1988**, 245, 223[CrossRef], [CAS]
33. Hammouche, M.; Lexa, D.; Momenteau, M.; Saveant, J. M. *J. Am. Chem. Soc.* **1991**, 113, 8455ACS Full Text, [CAS]
34. Paik, W.; Andersen, T.; Eyring, H. *Electrochim. Acta* **1969**, 14, 1217[CrossRef], [CAS]
35. Gattrell, M.; Gupta, N.; Co, A. *J. Electroanal. Chem.* **2006**, 594, 1[CrossRef], [CAS]
36. Schouten, K. J. P.; Kwon, Y.; van der Ham, C. J. M.; Qin, Z.; Koper, M. T. M. *Chem. Sci.* **2011**, 2, 1902[CrossRef], [CAS]
37. Jordan, J.; Smith, P. T. *Proc. Chem. Soc.* **1960**, 246[CAS]
38. Aylmer-Kelly, A.; Bewick, A. *Faraday Discuss. Chem. Soc.* **1973**, 56, 96[CrossRef], [CAS]
39. Hori, Y.; Murata, A.; Yoshinami, Y. *J. Chem. Soc., Faraday Trans.* **1991**, 87, 125[CrossRef], [CAS]
40. Hori, Y.; Murata, A.; Tsukamoto, T.; Wakebe, H.; Koga, O.; Yamazaki, H. *Electrochim. Acta* **1994**, 39, 2495[CrossRef], [CAS]
41. Hori, Y.; Koga, O.; Yamazaki, H.; Matsuo, T. *Electrochim. Acta* **1995**,

40, 2617[CrossRef], [CAS]
42. Amatore, C.; Saveant, J. M. *J. Am. Chem. Soc.* **1981**, 103, 5021ACS Full Text, [CAS]
43. Amatore, C.; Saveant, J. M. *J. Electroanal. Chem.* **1981**, 126, 1[CrossRef], [CAS]
44. Gennaro, A.; Isse, A. A.; Severin, M.-G.; Vianello, E.; Bhugun, I.; Saveant, J.-M. *J. Chem. Soc., Faraday Trans.* **1996**, 92, 3963[CrossRef], [CAS]
45. Toyoshima, I.; Somorjai, G. A. *Catal. Rev.* **1979**, 19, 105[CrossRef], [CAS]
46. Hori, Y.; Takahashi, R. *J. Phys. Chem. B* **1997**, 5647, 7075[ACS Full Text]